AIAA JOURNAL
Vol. 39, No. 2, February 2001

Microdynamic Characterization of Modal Parameters for a Deployable Space Structure

Michel D. Ingham* and Edward F. Crawley†
Massachusetts Institute of Technology, Cambridge, Massachusetts 02139

Results are presented from an experimental investigation of the microdynamics of deployable space structures. The dynamic response of a representative deployable truss at submicrostrain levels of vibration was characterized in terms of modal parameters. The test article was subjected to stepped-sine sweeps through its fundamental flexible modes over a range of excitation amplitudes. High-sensitivity piezoceramic strain sensors were used in conjunction with a lock-in amplifier to measure the truss response from tens of microstrain down to one nanostrain. The results show that the values of modal frequency and damping ratio are strain dependent at high response amplitudes and strain independent at low amplitudes. It is inferred that, at microdynamic levels of excitation, the internal loads needed to overcome the joint friction are not attained. The nonlinear mechanisms in the deployable structure are, thus, not activated, resulting in a linear truss response.

Introduction

THE hunt for Earthlike planets orbiting other stars has come to the forefront of the space community's interest. This is one of the primary objectives of NASA's Origins program, which will launch a number of space-based observatories, starting in the next decade. These missions will employ both connected interferometers and large aperture telescopes with adaptive mirrors. Because of the size constraints imposed by the payload bays of carrier spacecraft, these telescopes will undoubtedly require some form of on-orbit deployment mechanism, including joints or hinges, which will introduce nonlinearity to the structure.

The success of the Origins missions will hinge on whether positioning of the optical elements can be maintained to within fractions of the viewing wavelength. Consequently, any minute disturbance will pose a serious threat to the stability of the precision optical systems. The response of structures with nonlinear elements to such small disturbances has yet to be researched in depth.

The dynamics of a structure are often characterized in terms of modal parameters, which include the mode shapes, the resonant natural frequencies of the structure, and the level of damping associated with each resonance. Accurate estimates of these parameters are required to build and verify dynamic models of structural systems, which may be used to predict the behavior of the structure in response to a given disturbance, or to represent the structural plant in the design of a control system. Whereas much research has been done in the field of modal identification at standard levels of excitation, very little work has focused on the so-called microdynamic regime. This regime is of critical importance to current and future precision space structures, for which the vibration environment must be known (and controlled) down to nanometer level. The main objective of this research, therefore, is to characterize experimentally the dynamic response of a deployable truss at submicrostrain levels of vibration, in terms of its modal parameters.

Other recent work in the microdynamics field has been done by Warren and Peterson,[1] who performed an experimental characterization of the microdynamics of a prototype deployable telescope support structure. They discovered that abrupt changes in structural shape at the microdynamic level occur as a result of dynamically induced relaxation of strain energy stored by friction mechanisms within the structure. Hardaway and Peterson[2] have outlined a detailed methodology for ground-based microdynamic-level testing; application of this methodology led to the development of a test facility, which allows the characterization of the mechanics of deployed structures up to 3 m in size with nanometer resolution.

Ting and Crawley[3] characterized damping within an erectable truss structure, subject to microdynamic-level excitation. Their work, done on a tetrahedral interferometer testbed, showed that structural damping is independent of strain below 1 microstrain, and increases with strain above that level (see Fig. 1). One of the goals of the study documented in this paper is to verify their conclusion for deployable trusses, where behavior may be significantly altered by the frictional joint mechanisms required for deployment.

In this paper, the hardware used, procedures followed, and results obtained from the microdynamic modal parameter characterization experiment will be presented. The implications of this study on the design of future precision space structures will be addressed.

Hardware and Instrumentation

Middeck Zero-Gravity Dynamics Experiment (MODE) Truss Testbed

The testbed used for the modal parameter characterization experiment was the middeck zero-gravity dynamics experiment structural test article (MODE STA). Because the purpose of this work was to gain insight on the microdynamic mechanisms at work in a typical deployable structure, tests were only performed on the baseline configuration of the STA. The baseline configuration consists of two four-bay deployable truss modules connected by erectable truss members, forming a straight truss, nine bays long (Fig. 2). The MODE and MODE-Reflight programs studied the dynamics of these and other truss modules assembled in different configurations.[4–6] In both of these programs, the modal behavior of these truss configurations was investigated at standard dynamic levels. In particular, the effects of nonlinearities (due to the joint friction and slackening tension cables) on the modal parameters were investigated. These millimeter- to micrometer-level dynamics experiments also demonstrated that increased preload results in stiffening and decreased modal damping.

For the purpose of limiting the test matrix size, microdynamic characterization was only performed on the two lowest-frequency global modes of the structure, namely, the first torsion and bending modes. These two modes are illustrated in Fig. 3. The natural frequency corresponding to the first torsion mode is approximately 7.7 Hz, whereas the first bending mode is in the vicinity of 20.7 Hz. The conclusions drawn from the tests on these modes are assumed to apply to the higher modes, where similar dynamic mechanisms are excited.

A brief description of the testbed follows, with emphasis placed on the joints and mechanisms relevant to this microdynamic study. A more thorough description of the structure is available in Ref. 4.

Received 15 July 1999; revision received 27 July 2000; accepted for publication 1 August 2000.

*Graduate Research Assistant, Space Systems Laboratory, Department of Aeronautics and Astronautics. Student Member AIAA.

†Professor and Department Head, Space Systems Laboratory, Department of Aeronautics and Astronautics. Fellow AIAA.

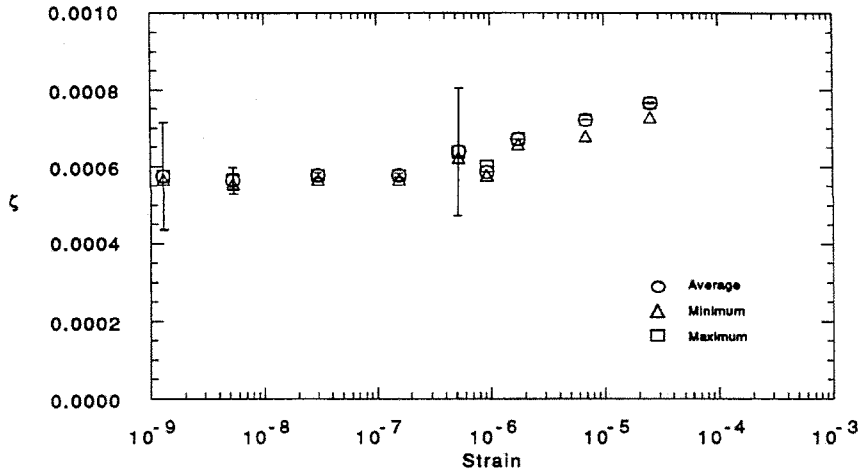

Fig. 1 Typical result from the microdynamic damping characterization of an erectable truss.[3]

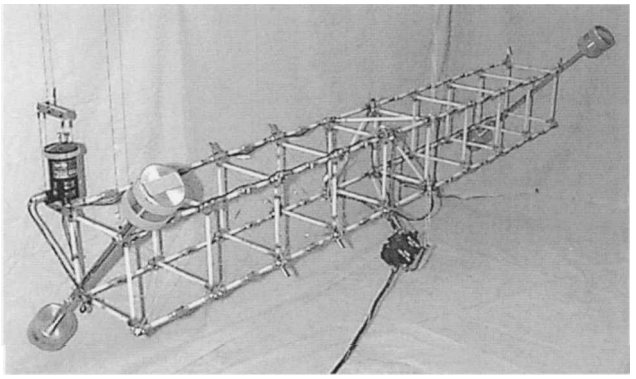

Fig. 2 MODE STA baseline configuration.

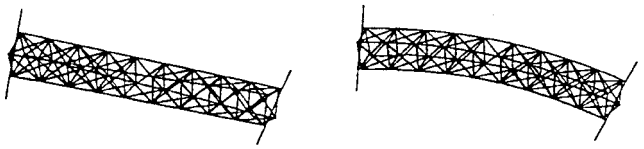

Fig. 3 First torsion and bending modes for the MODE STA.

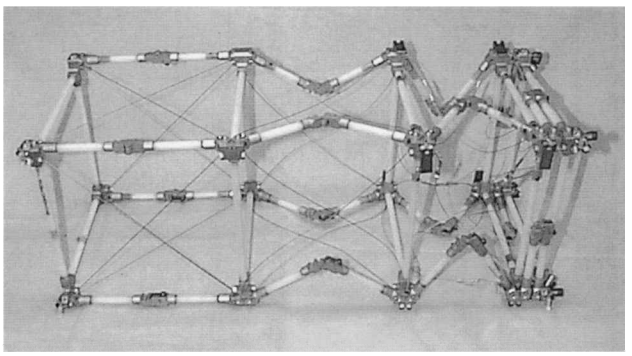

Fig. 4 Partially collapsed deployable module.

Two deployable truss modules form the bulk of the MODE baseline configuration. Each four-bay section weighs approximately 3 lb (1.4 kg), and measures 32 in. (81.3 cm) long in its deployed state. Each bay is cubic, 8 in. on a side. The Lexan longerons hinge at their midpoints and at the attachment points to the batten frames. The truss folds up in accordion fashion, with the batten frames remaining rigid (Fig. 4). As the longeron unfolds during the deployment process, the aluminum knee joint locks approximately 2 deg over center and

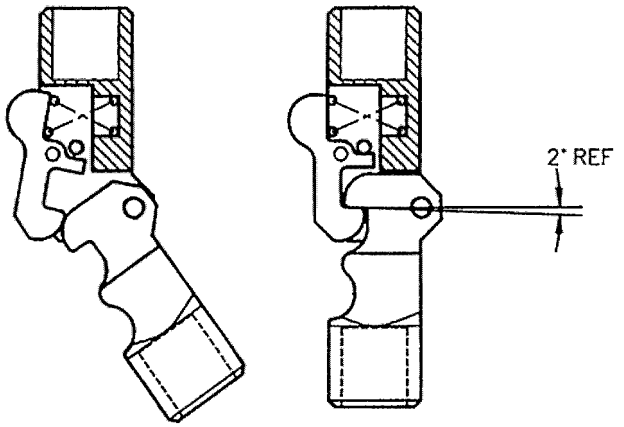

Fig. 5 Knee joint and latch mechanism.

is held by a latch mechanism, as shown in Fig. 5. The end lugs of the longerons, also made of aluminum, are hinged to the batten frame corner fittings.

The batten frames are made of four lengths of the same Lexan rods, connected with epoxy to four aluminum corner fittings. These fittings receive the pinned lugs of the longerons. The batten frames at either end of the deployable truss section have corner fittings with threaded holes, which allow connection with erectable truss members.

Each lateral face of each bay has a pair of crossing diagonal cables designed to preload the truss structure. These stranded stainless steel cables are known to exhibit nonlinear force-displacement behavior at standard levels of tensile strain. The cables have ball terminators, which sit in spherical receptacles in the batten frame corner fittings (Fig. 6). Approximately 28 lbf (125 N) of pretension are applied to the longerons when they are locked in their fully deployed state, at room temperature. This corresponds to roughly 50% of their estimated buckling load.

In the MODE baseline configuration, the two four-bay deployable sections are joined by a bay built from erectable truss members. There are four longerons and four diagonal truss members, all made of Lexan with aluminum end lugs.

The suspension system consists of four coil springs attached to ceiling-mounted brackets, connected to lengths of steel wire that drop to the four end nodes at the top of the STA. The overall length of the suspension system is 120 in. (3 m); at this length, the pendulum mode frequency is roughly 0.3 Hz. Rigid appendages, consisting of steel shafts with cylindrical steel masses at each end, are attached to the two end bays of the baseline truss (Fig. 2). Their original purpose was to lower the fundamental mode of the truss to approximately the correct scaled frequency of the space station solar arrays

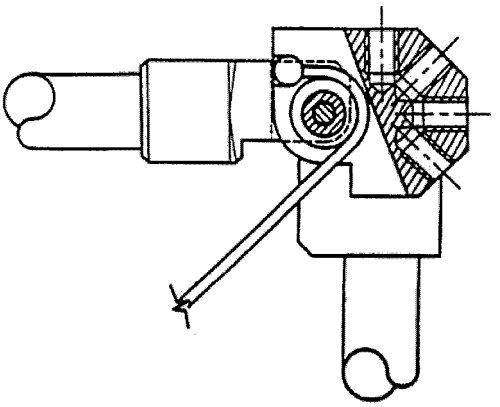

Fig. 6 Cable termination detail.

that the MODE STA was modeled after. They also provide the mass required to decrease the bounce mode of the suspension system to 1 Hz.

Actuators and Sensors

To provide the harmonic excitation for the majority of the microdynamic stepped-sine sweeps, a piezoceramic bending actuator was used. It was designed to satisfy the following requirements: no stiction at low excitation, and dynamic range wide enough to excite the truss at levels ranging from 0.05 lbf down to 1×10^{-6} lbf. The design of this actuator is discussed in greater detail in Ref. 7. Force measurements are provided by a load cell placed between the actuator and the structure.

For the three highest-amplitude tests on the truss bending mode, where load levels greater than 0.04 lbf were required, an electromagnetic proof-mass shaker was used. Note that substituting this actuator had a significant effect on the truss dynamics because its mass and inertia properties are quite different from those of the piezo bending actuator.

Piezoceramic (PZT-5A) strain gauges were chosen as sensors for this microdynamic characterization experiment because they satisfied the signal-to-noise and resolution requirements without being too bulky or prohibitively expensive to acquire. These sensors have been shown to have linear response down to a strain level of 10 picostrain.[8]

The gauges were bonded to the surface of two struts (one longeron and one diagonal) in the erectable center bay of the truss. The gauge on the diagonal offers high observability of the first torsion mode, whereas the bending mode is most observable from the gauge on the longeron.

The piezo gauges were calibrated against resistive strain gauges, which were bonded to the same truss members. Calibration was performed for each mode of the structure tested, for strains between 0.1 and 100 $\mu\varepsilon$. The voltage-to-strain relationship could then be extrapolated down to the nanostrain level. A typical value for the sensitivity is 1.5×105^5 V/ε (obtained for the torsion mode).

A lock-in amplifier was used to extract the content of the piezogauge output at the excitation frequency, in the presence of the significant noise floor encountered during the microdynamic measurements.

Test Procedure

For each of the torsion and bending modes of the truss, sets of stepped-sine sweeps were performed at two different amplitude levels per decade of strain, down to nanostrain level, for example, around 7, 2, 0.7, 0.2 microstrain, etc. The frequency increments were chosen small enough to represent the peak in the frequency response function accurately. Steps of 5×10^{-4} Hz were used for tests on the torsion mode, whereas larger steps of 4×10^{-3} Hz were allowed for the more highly damped bending mode.

Each set of sweeps was composed of six sweeps, alternating forward and backward, at a given excitation voltage amplitude. Each frequency change was followed by a 20-s wait, to allow the transients in the lock-in amplifier output to die out. After the wait time, the magnitude of the sensor output and phase with respect to the reference signal (excitation voltage from the function generator) were read and stored.

Generally, estimates of the modal parameters can be computed from transfer function data (in this case strain output to load input). However, for the two modes of interest, the load input was essentially constant over the frequency ranges of the sweeps. Therefore, the piezogauge output data were used directly to compute the modal parameters.

Data Reduction

Once the magnitude and phase data were acquired for a set of sweeps, the next step was to use the frequency response functions (FRFs) to obtain estimates for the modal parameters, f_n and ζ_n. To obtain the modal parameter estimates for the microdynamic characterization experiment, combinations of three methods were used for the different modes and amplitudes tested. The circle fit method[9] provided reasonable estimates for ζ_n for all of the data sets taken; therefore, this method was used exclusively to obtain the damping estimates. However, the natural frequency estimates obtained from the circle fit were inaccurate, due to the high sensitivity of the f_n estimate to unavoidable deviations from theoretical behavior.[7] Thus, instead, the natural frequency estimates were obtained using one of two other methods, depending on the quality of the data. For data taken at the higher strain levels (i.e., above 1 microstrain for the torsion mode and above 0.1 microstrain for the bending mode), there is very little noise contamination, that is, smooth FRF curves. Taking the frequency of the peak in these FRFs was a simple way to obtain f_n. As the strain level drops, the FRF data become noisier, making it difficult to identify the peak of the curve accurately. Thus, for the lower amplitudes (below 1 microstrain for the torsion mode and 0.1 microstrain for the bending mode), the f_n estimate was obtained by fitting an analytical single-degree-of-freedom (SDOF) resonance to the FRF magnitude data:

$$|\text{FRF}| = A \Big/ \left\{ \left[1 - (f/f_n)^2 \right]^2 + [2\zeta_n (f/f_n)]^2 \right\}^{\frac{1}{2}}$$

Precision and Accuracy of Measurements

In any experiment, there are limitations on the precision and accuracy of measured data. For microdynamic experiments, it is particularly important to identify and quantify these limitations, due to the high sensitivity of these types of tests to the disturbance environment. Accuracy is defined as the closeness of agreement between a measured value and a true value.[10] The total measurement error is composed of a systematic error component (due to sensor calibration imperfections, for example) and a random error component (often called repeatability, or precision error). To evaluate the level of precision error associated with this experiment, it was necessary to look at the scatter in the results, both within each set of six sweeps and between different sets at the same nominal excitation level. The amount of scatter in the results from one set of six sweeps was determined by comparing the maximum, minimum, and mean values of peak strain $\varepsilon_{\text{peak}}$, natural frequency f_n, and damping ratio ζ_n. As another indication of the scatter within a set, the standard deviation in each of these values was computed. Another measure of repeatability was obtained by comparing results from different sets of sweeps at the same excitation level, performed on different days.

For modal parameter characterization in the microdynamics regime, several potential sources of error can be identified: aerodynamic effects, transmission of mechanical vibration through the suspension system and wiring, acoustic effects, electrical noise, actuator and sensor dynamics, temperature effects, and humidity effects. Error can also be associated with the data reduction procedure because it relies heavily on accurate least-square fits to the data. A thorough discussion of each of these error sources is found in Ref. 7. Two of these sources are singled out as the most significant contributors to imprecision or inaccuracy in the results from this experiment: transmission of mechanical vibration and electrical noise. The effects of the other sources are assumed negligible on the resulting modal parameter estimates.

Transmission of Mechanical Vibration

The first important source of error is the transmission of vibration disturbances through the suspension system and the electric wires leading from the sensors and actuator. Based on the isolation characteristics of the suspension system, the levels of vibration transmitted through the suspension wires would be negligible for traditional modal parameter characterization tests; for microdynamic-level tests, however, these vibrations are not insignificant. The noise floor encountered in the piezogauge output, after filtering by the lock-in amplifier, was on the order of 1 nanostrain rms. Transmission of mechanical vibration through the suspension is identified as a likely contributor to the baseline noise level.

The suspension system also presents a path for energy to leave the system, which results in inaccuracy in the damping measurement. An estimate of this effect's contribution to the total damping ratio can be obtained by computing the ratio of energy lost in the springs during one vibration cycle to the total strain energy of the truss. The damping due to energy lost through the suspension is estimated to be at least an order of magnitude lower than the total measured damping.

Aside from the suspension system, the wires running to the sensors and actuator provide the only other physical connection between the truss and the laboratory environment. Care was taken to minimize the effects of wires on the truss dynamics; this is of particular importance given the small levels of vibration observed in this experiment. All of the wires running to the actuator and from the piezogauge sensors were secured away from the structure and slackened sufficiently to minimize their boundary condition effect at the points of attachment to the truss.

Electrical Noise

Given the low levels of signal involved in microdynamic experimentation, all signal-carrying wires were properly insulated, and ground loops were avoided. The gauges and lead wires were covered with an insulating layer of silicon rubber sealant to reduce the effects of electrical cross talk. To minimize signal loss along the transmission path, all wire lengths were kept as short as possible. Despite the efforts made to minimize electrical noise, it is considered the other likely contributor to the noise floor in the output from the piezogauge, along with transmission of mechanical vibration to the structure.

Experimental Results

For each of the two modes of interest in the experiment, FRFs were measured at various strain amplitudes between 0.1 millistrain and 1 nanostrain. A considerable amount of data was collected from the stepped-sine sweep tests. For the sake of conciseness, data from only a few representative sweeps are identified in this paper; the final results of the modal parameter characterization are presented in graphical form. The complete data set can be found in Ref. 7.

Sweep Results: Torsion

In Fig. 7, the piezogauge output FRFs for one set of representative sweeps over the torsion mode, at the higher end of the microdynamic range, are overlaid. The average peak response of the truss over the six sweeps in the set was 15.8 microstrain. A qualitative measure of the repeatability within a set of sweeps can be inferred from how well the sweeps overlay. In this case, some spread is seen in the data on either side of the peak: sweeps performed in opposite directions (i.e., increasing vs decreasing frequency) tended to follow slightly different curves. This type of hysteretic behavior is attributed to nonlinearity in the torsion mode at the higher amplitude levels. Such nonlinearity may arise due to load cycling of the stranded diagonal cables or of the numerous frictional interfaces in the structure joints caused by the torsional motion of the truss.

The FRF magnitude data from the first sweep in the set are plotted in Fig. 8. The modal peak presents an obvious nonlinearity: It is shown to be skewed toward the low-frequency side but not so much that it exhibits jump behavior in its frequency response. The dashed line on the plot corresponds to the SDOF resonance fit. The nonlinearity in the first torsion mode prevents a good fit to the linear

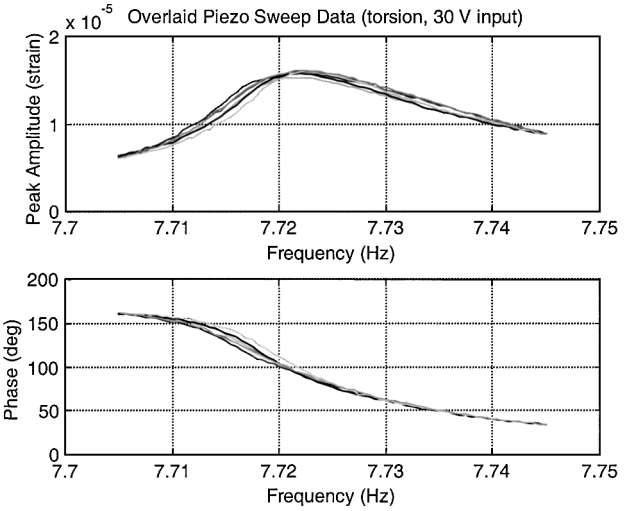

Fig. 7 Typical piezo-output data (torsion mode, microstrain level); phase measurement is taken with respect to the signal generator voltage.

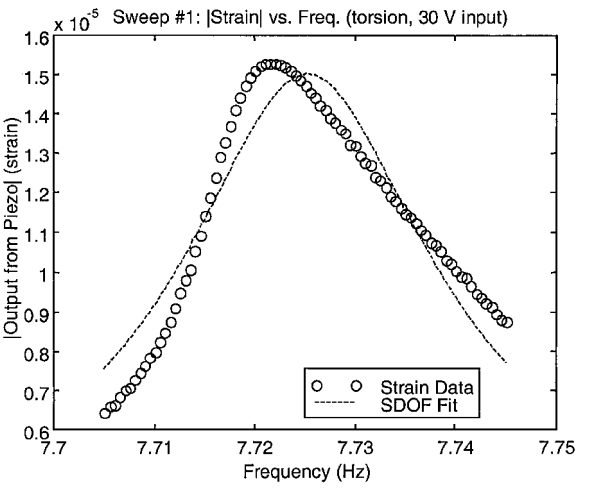

Fig. 8 Typical piezo-output sweep data (torsion mode, microstrain level).

SDOF model. The estimate for natural frequency was, therefore, chosen as the frequency of the peak FRF amplitude, 7.722 Hz.

Figure 9 shows a polar plot of the FRF data from the same representative microstrain-level sweep over the torsion mode. The circle fit to the data points appears to be unaffected by the aforementioned nonlinearity. As explained in the description of the circle fit method given by Ewins,[9] damping ratio estimates are obtained for each pair of FRF data points consisting of one point with frequency above f_n and one point with frequency below f_n. This yields a matrix of damping estimates. Ideally, all of the estimates should be identical; in reality, the mean value is taken as the actual damping ratio for the mode. By looking at the deviation from the mean of all of the estimates, an indication of the quality of the circle fit analysis is obtained. Figure 10 shows the scatter in the matrix of damping estimates for the sample microstrain-level torsion data, plotted as a function of the frequency above f_n and the frequency below f_n. The damping estimates from the circle fit characterization technique are scattered by as much as $\pm 40\%$ about the mean ζ_n (evaluated at 0.0014), whereas the surface in the scatter plot remains relatively smooth. This systematic variation in the damping estimates is indicative of the nonlinear behavior in the torsion mode.

The FRF magnitude data from one typical nanostrain-level sweep (average peak strain of 7.5 nanostrain) are plotted in Fig. 11. The SDOF model fits well to these low-amplitude FRF data, yielding a natural frequency estimate of 7.745 Hz. Evidently, the torsion

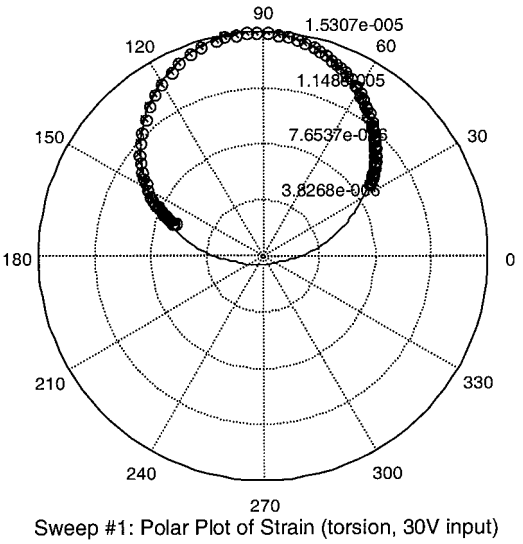

Fig. 9 Typical circle fit to piezo-output (torsion mode, microstrain level).

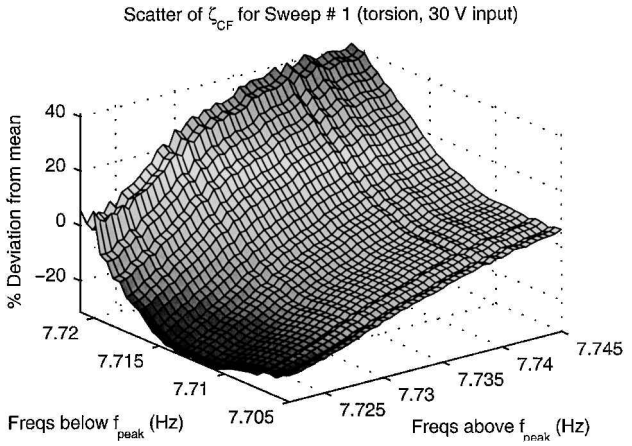

Fig. 10 Typical scatter of damping from circle fit to piezo-output (torsion mode, microstrain level).

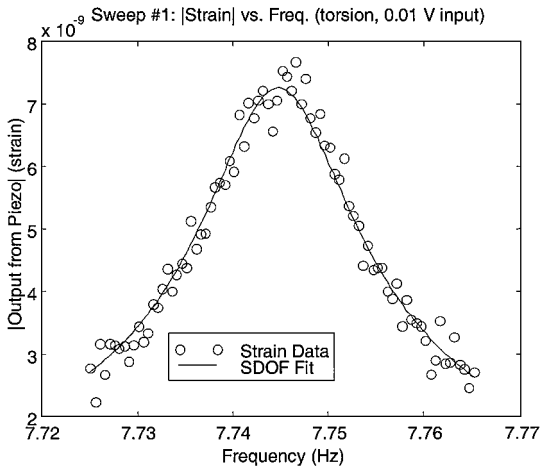

Fig. 11 Typical piezo-output sweep data (torsion mode, nanostrain level).

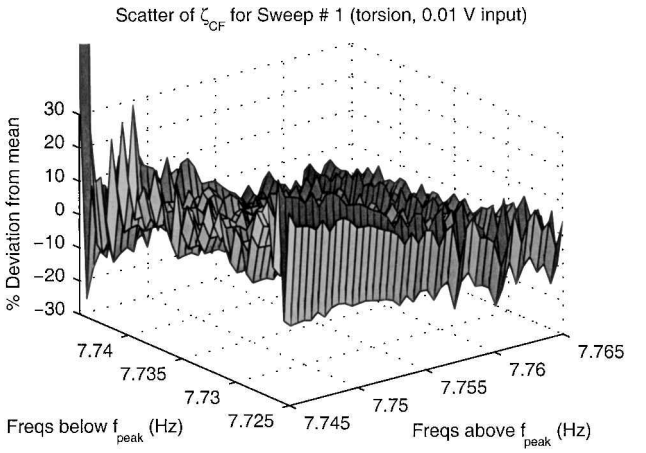

Fig. 12 Typical scatter of damping from circle fit to piezo-output (torsion mode, nanostrain level).

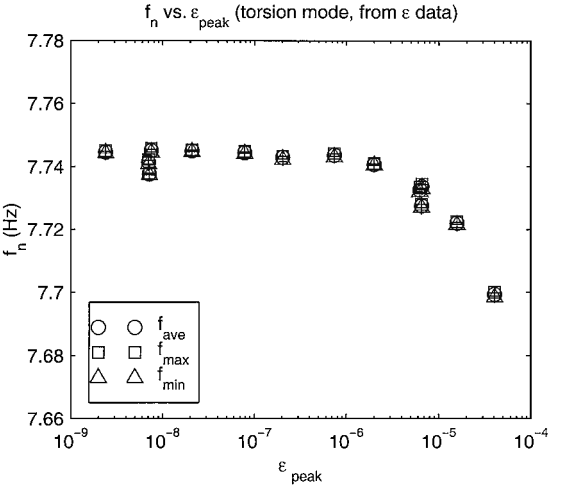

Fig. 13 Natural frequency estimates vs strain amplitude (torsion mode).

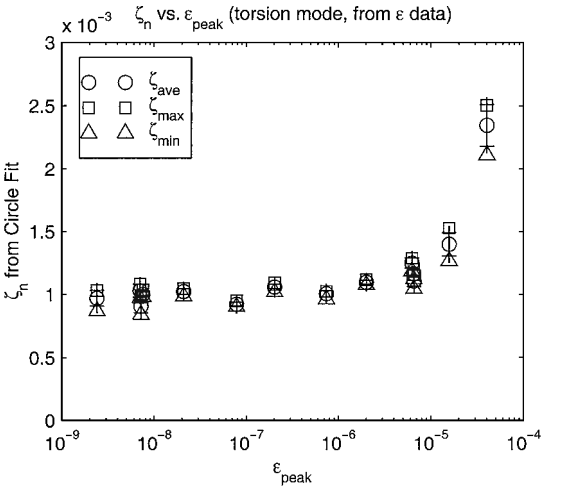

Fig. 14 Damping ratio estimates vs strain amplitude (torsion mode).

mode becomes linear as excitation amplitude is decreased. Compared to the higher-amplitude data, the slightly sharper peak in the low-amplitude FRF indicates that the level of damping has decreased, whereas the natural frequency estimate has increased by more than 0.02 Hz. The circle fit procedure results in a mean ζ_n estimate of 0.001. The scatter in the damping ratios from the circle fit procedure lies predominantly within $\pm 10\%$ of the mean ζ_n (Fig. 12). Compared to the corresponding microstrain-level scatter plot (Fig. 10), the surface is less steep and exhibits random rather than systematic variation, which is consistent with the increased linearity and noise in the data.[9]

The results from all of the microdynamic tests on the torsion mode are presented graphically, in the form of f_n vs $\varepsilon_{\text{peak}}$ (Fig. 13) and ζ_n vs $\varepsilon_{\text{peak}}$ (Fig. 14) plots. In these plots, the mean value of the modal parameter estimates from each set of six sweeps is plotted as a circle. The maximum and minimum values from each set of sweeps are represented as squares and triangles, respectively. The standard

deviation of the six sweeps in each set was computed as well. The error bars on the plots correspond to one standard deviation above and below the mean value.

Below a strain level of 1 microstrain, the torsion mode of the structure behaves linearly. Figure 13 shows the natural frequency estimates flattening out at a value of approximately 7.745 Hz and the damping ratio asymptoting to a value of roughly 0.001. Above 1 microstrain, the torsion mode exhibits softening nonlinear behavior, with f_n decreasing to 7.7 Hz at the highest strain level tested. The corresponding ζ_n increases to a level of 0.0024 at this amplitude.

Good precision was achieved in all of the natural frequency estimates, judging by the close proximity of the maximum and minimum values to the mean and the insignificant size of the error bars in Fig. 13. The standard deviation values are all smaller than 0.02% of their corresponding mean values. As far as the damping estimates are concerned, the best precision was achieved in the range of strains between 7.5 nanostrain and 6.3 microstrain: The standard deviations in ζ_n for these sets of sweeps correspond to less than 5% of the mean values obtained. At the lowest strain level tested (2.4 nanostrain), the standard deviation of the ζ_n estimates increased to roughly 7% of the mean ζ_n, due to significant noise in the data. At the two highest amplitude levels (15.8 and 40.4 microstrain), the same hysteretic nonlinearity that caused the forward and backward sweeps not to overlay (Fig. 7) results in decreased precision in the damping estimates, amounting to a standard deviation of roughly 7% of the mean ζ_n.

In addition to the measures of precision available within each set of sweeps, a measure of the repeatability between sets of sweeps performed on different days was sought. To this end, tests on the torsion mode were repeated twice, at two strain amplitude levels (6.3 microstrain and 7.5 nanostrain). The modal parameter estimates from these repeatability tests are plotted with the original results in Figs. 13 and 14. The mean values of $\varepsilon_{\text{peak}}$, f_n, and ζ_n from the repeated tests were found to lie within 6.5, 0.05, and 11.5% of their respective original mean values.

Sweep Results: Bending

Figure 15 presents the FRF magnitude data from a typical sweep performed over the first bending mode of the truss, at the higher amplitude end of the microdynamic regime. The electromagnetic proof-mass shaker was used to excite the bending mode of the structure to a measured peak strain of approximately 1.1 microstrain. The SDOF model is seen to fit the data reasonably well. Only slight nonlinearity is detected, barely tilting the peak toward the low frequencies. The natural frequency estimate is read off as the frequency of the peak in the data (20.740 Hz). The damping estimates obtained from the circle fit characterization exhibit only slight systematic variation, staying within ±10% of the mean ζ_n, evaluated at 0.0023. This is consistent with predominantly linear behavior.

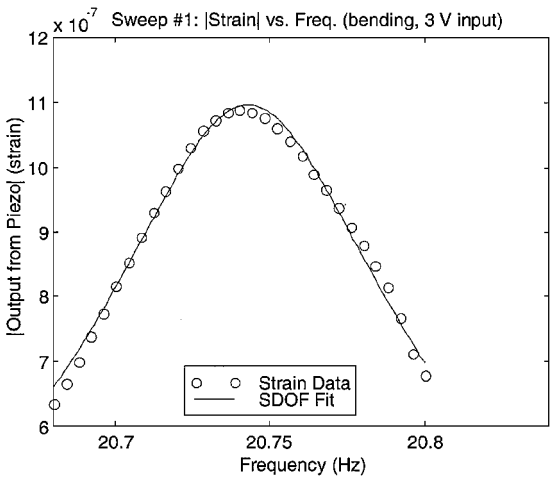

Fig. 15 Typical piezo-output sweep data (bending mode, microstrain level).

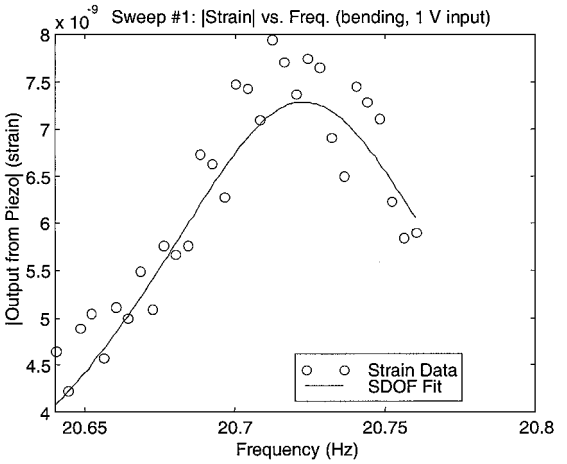

Fig. 16 Typical piezo-output sweep data (bending mode, nanostrain level).

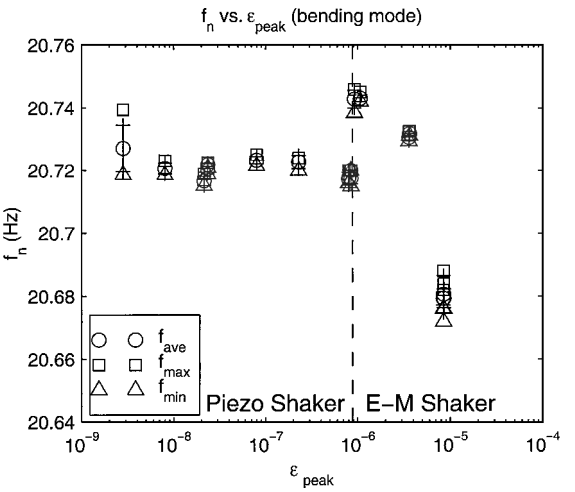

Fig. 17 Natural frequency estimates vs strain amplitude (bending mode).

FRF magnitude data from a representative nanostrain-level sweep are shown in Fig. 16. For this low amplitude, the piezo bending actuator was used to apply the sinusoidal load. The peak strain attained was 8 nanostrain. Because of the noise in the data, it is difficult to judge the quality of the SDOF resonance fit. Nonetheless, it would appear that the fit provides a decent estimate of the natural frequency. The f_n estimate from this sweep is 20.721 Hz. The circle fit to the FRF data yields a damping ratio of 0.0025 for the bending mode. The noise-induced scatter in the damping estimates generally lies within ±20% of the mean ζ_n.

The results from all bending mode tests are presented graphically in Figs. 17 and 18. As was done for the torsion mode results, the mean, maximum, and minimum values of each modal parameter estimate are plotted. The error bars extend one standard deviation above and below the mean value.

The transition between the two different actuators causes discontinuities in the plots of f_n vs $\varepsilon_{\text{peak}}$ and ζ_n vs $\varepsilon_{\text{peak}}$ around the 1-microstrain mark. The difference in inertial properties between the two shakers is identified as the reason for the significant jump seen in the plot of f_n vs $\varepsilon_{\text{peak}}$. Despite these discontinuities, both plots exhibit the general trend of linearity at strain amplitudes below 1 $\mu\varepsilon$ and softening nonlinearity at higher amplitudes. Figure 17 shows that the natural frequency of the bending mode remains essentially constant at low amplitudes, at approximately 20.72 Hz based on the piezobender actuator tests. The tests with the electromagnetic shaker show the natural frequency asymptoting toward a frequency around 20.75 Hz. The damping ratio estimates decrease as amplitude decreases, until a low-amplitude limit of roughly 0.0025 is reached.

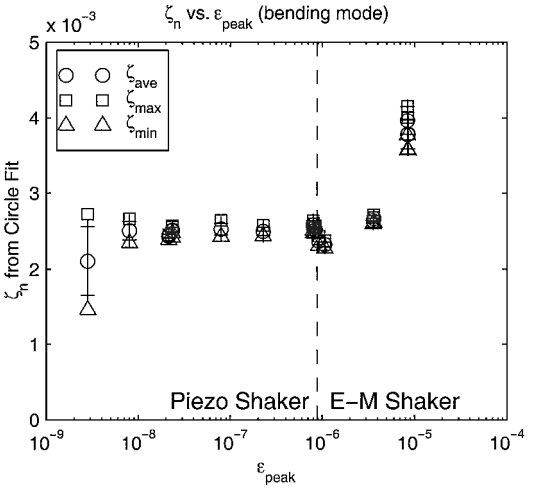

Fig. 18 Damping ratio estimates vs strain amplitude (bending mode).

Although the mean parameter estimates for the lowest strain amplitude (2.8 nanostrain) seem to diverge slightly from the aforementioned trends, note that the accuracy of these estimates is suspect because of systematic fitting errors induced by excessive noise in the data. Nonetheless, the low-amplitude parameter values predicted by the trends lie within the scatter of the lowest-amplitude results.

In general, reasonable precision was achieved in the bending mode tests, as judged by the limited scatter in the parameter estimates within each set of sweeps. For all strain amplitudes tested, other than the lowest, the standard deviation in the frequency estimates was 0.0021 Hz or better. The worst-case precision achieved in the f_n estimates was for the lowest amplitude tested (2.8 nanostrain), where the data were corrupted by noise. The standard deviation of these six estimates rose to 0.0075 Hz. As for the damping ratio estimates, the standard deviations for all but the lowest amplitude tests are less than 5% of the mean ζ_n values. The standard deviation of the damping ratio estimate from the lowest amplitude tests was found to be 4.5×10^{-4}, or 22% of the mean ζ_n.

Repeatability tests were performed at two strain amplitudes excited with the piezobending actuator (23 nanostrain and 0.8 microstrain) and at all three amplitudes excited with the electromagnetic shaker (1, 3.6, and 8.5 microstrain). These repeated modal parameter estimates are plotted with the original results in Figs. 17 and 18. All of the mean values of $\varepsilon_{\text{peak}}$, f_n, and ζ_n from the repeated tests were found to lie within 13, 0.02, and 5% of their original mean values, respectively.

Implications for Future Precision Space Structures

The structural requirements for future space telescopes (from NASA's Origins program) will present a challenging packaging problem. For example, plans for the Space Interferometry Mission (SIM) call for an Earth-orbiting interferometer that must deploy to a baseline length on the order of 10 m. To accomplish its lofty astrometry and imaging goals, the distance between the telescopes on the deployed beamlike SIM structure must be kept stable to within 10 nm, that is, on the order of nanostrain.[11] Clearly, results from microdynamic studies may have important implications on the design of this type of precision space structure.

One important finding is that, for space structures operating in the microdynamic regime, damping decreases to levels significantly lower than those seen at higher dynamic amplitudes. Such low damping levels may be relevant to spacecraft such as SIM, whose operations will impose strict quiescence requirements on the structure. These levels of damping should be considered in the dynamic modeling of the spacecraft and may factor into the design of the isolation stages for the sensitive instrumentation.

From another perspective, the results from the microdynamic modal parameter investigation can be seen as positive for precision space structures such as SIM: This work indicates that linearity of a structure is approached at low levels of vibration, which will greatly simplify the microdynamic modeling task. Along with the Ting and Crawley[3] work on an erectable structure, these findings represent two data points confirming linear behavior in the modal parameters at low strain. Despite that both experiments pointed to a linear/nonlinear transition occurring around 1 microstrain, the actual response level for which transition occurs is certainly mechanism dependent, in general. For structures featuring different types of joints and made from other materials, the critical strain response level may well change.

Conclusions

Based on the results from the microdynamic modal parameter characterization experiment, some interesting conclusions can be drawn. These tests showed nonlinear softening behavior for strain response levels above 1 microstrain but essentially linear behavior below 1 microstrain, that is, constant values for natural frequency and damping ratio are approached below this critical response level. From this result, it is inferred that the nonlinear structural mechanisms, which dominate the damping at high excitation levels, are not activated at low excitation levels; the underlying linear dissipation mechanisms become the main source of structural damping. This result was common to both bending and torsion modes, despite that the dynamic mechanisms involved in these structural modes are quite different: longeron extension and compression in the case of the bending mode vs bay shearing in the case of the torsion mode. This points to a certain degree of universality in the microdynamic behavior of nominally nonlinear structures. Although the actual source of the linear damping limit was not identified, it is assumed to be dictated by material damping and perhaps also linear dissipation mechanisms within the joints.

As mentioned earlier, a similar microdynamic investigation was performed by Ting and Crawley[3] on an erectable truss structure. Their experiments focused on the characterization of damping within a tetrahedral truss structure, for strain levels from 10^{-9} up to 10^{-4}. By comparing results from the Ting and Crawley experiments and the microdynamic tests on the MODE STA, it was hoped that some conclusions could be drawn regarding the similarities and/or differences in the microdynamic behavior of erectable vs deployable truss structures. Typical results from the Ting and Crawley experiments were presented in Fig. 1. Figure 1 shows the damping ratio estimates vs strain amplitude for one mode of the structure. Familiar trends were observed in those experiments: the small strain range was evidently dominated by linear damping mechanisms, that is, constant ζ_n, whereas the large strain range exhibited nonlinear damping behavior (increasing ζ_n with increasing $\varepsilon_{\text{peak}}$). The strain amplitude at which this transition occurred was around 1 microstrain, the amplitude at which linear-to-nonlinear transition occurred in the microdynamic tests on the MODE STA. Note that certain other modes tested by Ting and Crawley did not exhibit any significant nonlinear behavior at all. Their damping ratios were found to be essentially constant over the entire strain range tested. The main conclusion drawn from the comparison of the two experiments is that, despite the presence of significantly more nonlinear mechanisms in a deployable structure, a lower limit in damping is reached nonetheless, once the vibration levels become small enough.

Acknowledgments

This research was sponsored by the Jet Propulsion Laboratory (JPL) at the California Institute of Technology. The authors greatly appreciate the support of Marie Levine, the project Technical Monitor at JPL. This paper was originally presented as Paper IAF-98-I.2.01 at the International Astronautical Federation Congress, Melbourne, Australia, 29 September–3 October 1998.

References

[1] Warren, P. A., and Peterson, L. D., "Submicron Mechanical Stability of a Prototype Deployable Space Telescope Support Structure," AIAA Paper 97-1375, April 1997.

[2] Hardaway, L. M. R., and Peterson, L. D., "Ground-Based Microdynamic Testing of Deployed Optical Structures," AIAA Paper 99-1273, April 1999.

[3]Ting, J. M., and Crawley, E. F., "Characterization of Damping of Materials and Structures from Nanostrain Levels to 1000 Microstrain," *AIAA Journal*, Vol. 30, No. 7, 1992, pp. 1856–1863.

[4]Crawley, E. F., Barlow, M. S., van Schoor, M. C., Masters, B., and Bixos, A. S., "Measurement of the Modal Parameters of a Space Structure in Zero Gravity," *Journal of Guidance, Control, and Dynamics*, Vol. 18, No. 3, 1995, pp. 385–394.

[5]Barlow, M. S., "Modeling and Ground Modal Identification of Space Structures," S.M. Thesis, Dept. of Aeronautics and Astronautics, Massachusetts Inst. of Technology, Cambridge, MA, Jan. 1992.

[6]Bobronnikov, S. V., "Modeling and Modal Identification of Jointed Space Structures in One- and Zero-Gravity Environments," S.M. Thesis, Dept. of Aeronautics and Astronautics, Massachusetts Inst. of Technology, Cambridge, MA, Sept. 1994.

[7]Ingham, M. D., "Microdynamics and Thermal Snap Response of Deployable Space Structures," S.M. Thesis, Dept. of Aeronautics and Astronautics, Massachusetts Inst. of Technology, Cambridge, MA, June 1998.

[8]Forward, R. L., "Picostrain Measurements with Piezoelectric Transducers," *Journal of Applied Physics*, Vol. 51, No. 11, 1980, pp. 5601–5603.

[9]Ewins, D. J., *Modal Testing: Theory and Practice*, Wiley, New York, 1984, pp. 158–168.

[10]Coleman, H. W., and Steele, W. G., *Experimentation and Uncertainty Analysis for Engineers*, 2nd ed., Wiley, New York, 1999, p. 6.

[11]Allen, R. J., Peterson, D., and Shao, M., "Space Interferometry Mission—Taking Measure of the Universe," *Optical Telescopes of Today and Tomorrow: Proceedings of the International Society for Optical Engineering*, Vol. 2871, edited by A. L. Ardeberg, Society of Photo-Optical Instrumentation Engineers, Bellingham, WA, 1997, pp. 504–515.

A. Berman
Associate Editor